


Communication

Heavy Alkyl-Benzene Sulfonate-Controlled Growth of Aragonite-Based Polymorphic CaCO₃ Crystals in Emulsion

Weiwei He ¹, Junqing Hu ², Weihao Sun ², Jiqiong Liu ³, Hongguang Guo ³, Changming Zhao ³, Qingguo Wang ³, Xiangbin Liu ^{3,4}, Meng Cai ³ and Weiguang Shi ^{4,5,*} ¹ School of Mechatronic Engineering, Daqing Normal University, Daqing 163712, China; vivian820626@163.com² No. 2 Oil Production Factory of Daqing Oilfield Ltd., Daqing 163414, China; hujunqing@petrochina.com.cn (J.H.); sunweihao@petrochina.com.cn (W.S.)³ Oil Production Engineering Research Institute of Daqing Oilfield Ltd., Daqing 163453, China; liujiqiong@petrochina.com.cn (J.L.); guohongg@petrochina.com.cn (H.G.); zhaochangming@petrochina.com.cn (C.Z.); wqg@petrochina.com.cn (Q.W.); liuxiangbin@petrochina.com.cn (X.L.); cyycaimeng@petrochina.com.cn (M.C.)⁴ College of Chemistry & Chemical Engineering, Northeast Petroleum University, Daqing 163318, China⁵ Key Laboratory of Continental Shale Hydrocarbon Accumulation and Efficient Development, Ministry of Education, Northeast Petroleum University, Daqing 163318, China

* Correspondence: sswwg2003@126.com

Abstract: The non-natural mineralization of CaCO₃ with special structures or morphologies is generated during the migration of crude oil and is the main form of scale in alkaline/surfactant/polymer (ASP) flooding in oilfields, adversely affecting oil recovery and causing environmental pollution. To date, the mineralization of aragonite superstructures and the role of heavy alkyl-benzene sulfonate (HABS) in mineralization are still unclear. In this work, aragonite-based superstructures of CaCO₃ crystals were obtained in an O/W emulsion with HABS to help deepen the understanding of the diversified growth of CaCO₃ scaling in oilfields. As a result, rosette-like, bouquet-like, and dumbbell-shaped CaCO₃ crystals with vaterite–aragonite, aragonite, and calcite–aragonite phases were formed with 200 mg/L HABS concentration at 45 °C for 60 min and spherical vaterite phase stabilized at a high HABS concentration (800 mg/L and 1000 mg/L). Rhombohedral calcite content experienced a fluctuation of about 40% as the HABS concentration varied. Needle-like and bundle-like aragonite precipitates were generated with increasing temperatures from 65 °C to 85 °C. Thus, HABS affects the nucleation and growth of the precipitated CaCO₃ solid, leading to modifications in the structure and morphology of the crystals. The synergistic effect between HABS and temperature can regulate ion pairs with the calcium ions and block sites that are essential to the incorporation of new solutes into the crystal lattice, which leads to the heterogeneous nucleation of vaterite and aragonite on calcite, forming aragonite-based superstructures in kerosene emulsion. This work may enrich the understanding of CaCO₃ mineralization in oilfields, and also provide a novel strategy for manufacturing organic–inorganic composites.

Keywords: aragonite; HABS; polymorphic crystals; superstructure; mineralization; kerosene emulsion

Citation: He, W.; Hu, J.; Sun, W.; Liu, J.; Guo, H.; Zhao, C.; Wang, Q.; Liu, X.; Cai, M.; Shi, W. Heavy Alkyl-Benzene Sulfonate-Controlled Growth of Aragonite-Based Polymorphic CaCO₃ Crystals in Emulsion. *Crystals* **2023**, *13*, 1107. <https://doi.org/10.3390/cryst13071107>

Academic Editors: Waldemar Maniukiewicz and Carlos Rodriguez-Navarro

Received: 15 June 2023

Revised: 11 July 2023

Accepted: 14 July 2023

Published: 16 July 2023



Copyright: © 2023 by the authors. Licensee MDPI, Basel, Switzerland. This article is an open access article distributed under the terms and conditions of the Creative Commons Attribution (CC BY) license (<https://creativecommons.org/licenses/by/4.0/>).

1. Introduction

As an abundant mineral in the world, CaCO₃ has attracted tremendous attention due to its numerous morphologies and polymorphs [1–4]. To date, studies have shown that CaCO₃ has seven phases, including amorphous calcium carbonate (ACC) [5], calcium carbonate monohydrate (monohydrocalcite) [6], calcium carbonate hexahydrate [7], rhombohedral calcite [8], orthorhombic aragonite [9] and hexagonal vaterite [10], as well as the newly discovered phase, calcium carbonate hemihydrate [11]. In addition, CaCO₃ or CaCO₃-based materials have significant applications, especially in bone regeneration and drug delivery due to their excellent biocompatibility [12,13]. However, CaCO₃ can

exist in different morphologies and crystal structures, and some of them might result in scaling, reducing oil recovery in oilfields. In addition, the scaling phenomenon is common in industrial production processes, such as circulating cooling water systems and pipe flow systems [14]. The details of these scaling processes and the exact role played by polymorphic CaCO_3 have not been identified.

Aragonite, as a high-temperature, metastable polymorph of CaCO_3 , usually exists in the form of needle-like crystals. It is the main constituent in many sea shells and corals and can also form inorganically in warm shallow seas [15]. In addition, aragonite is also an ideal reinforcement composite material due to its particular structure and is an important biomineral [16]. For this purpose, the ability to selectively control the formation of this material has become a hot research topic. Hence, a number of approaches have been developed to control the morphology of aragonite crystals into, e.g., nanofilament networks [17] or tablet-like [18], needle-like and dandelion-like superstructures [19,20]. In China's Daqing oilfield, a ubiquitous polycrystalline CaCO_3 phase with spherical, rod-like, flower-like and radiate fan-like morphologies, among others, is observed [21]. Although aragonite exhibits various morphologies, the formation of a dumbbell-like aragonite superstructure mixed with rhombohedral calcite in the Daqing oilfield is a unique phenomenon that requires further investigation into the crystal growth mechanisms involved. The oriented dissolution of calcite and the epitaxial growth of aragonite may play a crucial role in the formation of this structure. Only Jing has reported that partially hydrolyzed polyacrylamides can lead to a change in the formation rate of vaterite or aragonite nuclei, as well as a change in the morphology of aragonite to be needle-like and leaf-like, which may be because the carboxyl groups in polyacrylamides molecules and Ca^{2+} in solution form chelates via coordination bonds, with these chelates then being adsorbed on the calcium carbonate surfaces of solid–liquid interfaces [22,23]. However, more research is needed to fully understand the processes involved in the oilfield and how they contribute to the formation of the observed morphology. In our previous research, labyrinth-like calcite crystals were synthesized in an HPAM–HABS hybrid system (HPAM: partially hydrolyzed polyacrylamide; HABS: heavy alkylbenzene sulfonate; these represent the two main constituents in ASP flooding in oil fields) [24]. However, the regulating effect of HABS in the formation of aragonite and mixed CaCO_3 crystals in emulsion systems is still unclear. Compared to the water phase, oil/water interfaces provide a unique non-equilibrium reaction environment with high surface energy and determine the transporting behavior of ions and/or molecules across the outer surroundings. This leads to the synthesis of novel structural nanomaterials via complex crystallization processes and furthers our knowledge about CaCO_3 scaling.

Herein, we reported a simple synthesis method of mixed aragonite with special morphology by applying the “one-step precipitation method” in a 20 V% O/W HABS/kerosene emulsion. During this process, various reaction conditions, including temperature, reaction time and the concentration of HABS, were investigated to obtain different crystal forms of calcium carbonate with multiple morphologies. The transformations of these CaCO_3 crystals is controlled by the coupling between the dissolution of calcite or vaterite that releases chemical species into the water phase and the precipitation of new aragonite, with the coupled process being driven by a synergistic effect between HABS and the temperature in kerosene emulsion. Thus, understanding the factors that influence crystal growth and morphology can help researchers develop new materials with specific properties and applications. In addition, our research may provide a HABS-stabilized interface for the oriented growth of CaCO_3 crystals and represent a similar environment to crude oil transportation, thus offering a successful remediation strategy to deal with carbonate scale in oilfields.

2. Materials and Methods

2.1. Materials

Calcium chloride (CaCl_2 , AR grade) and sodium carbonate (Na_2CO_3 , AR grade) were purchased from Tianjin chemical reagent factory. Heavy alkyl-benzene sulfonate (HABS, average molecular mass: 400–430 Da) was obtained from Daqing Donghao Investment Co.,

Ltd. (Daqing, China). Kerosene, purchased from Shanghai Aladdin biochemical technology Co., Ltd. (Shanghai, China), and was used in the oil phase, the purity of which exceeds 99%. All the above reagents were obtained from commercial sources and used as received without further purification. Deionized water was used to prepare aqueous solutions of CaCl_2 and Na_2CO_3 just before crystallization experiments and was made in our laboratory.

2.2. Preparation of CaCO_3 Crystals

Aqueous solution of CaCl_2 (0.04 mol/L, 250 mL), aqueous solution of Na_2CO_3 (0.04 mol/L, 250 mL) and a certain concentration of HABS were prepared beforehand. Calcium carbonate products were precipitated by quickly pouring 25 mL aqueous solution of Na_2CO_3 and a certain concentration of HABS into a 200 mL beaker containing a fixed volume content of kerosene (20 v%) with 25 mL CaCl_2 solution, followed by distilled water with various volume content (total volume: 100 mL). The mixture was then rapidly stirred for 10 min (1000 rpm) and agitated with a magnetic stirrer (30 rpm) for 5 min to 1 h, providing different reaction conditions. The HABS-controlled kerosene emulsion is an O/W-type emulsion. The resulting precipitates were filtered and washed thoroughly with distilled water. Finally, the product was dried in the oven at 45 °C for 24 h and used for further measurements.

The effects of reaction conditions on crystals were observed, including temperature (35 °C, 45 °C, 55 °C, 65 °C, 75 °C and 85 °C), reaction time (5 min, 10 min, 20 min, 30 min and 60 min) and the concentration of HABS (200 mg/L, 400 mg/L, 600 mg/L, 800 mg/L and 1000 mg/L).

The electrical conductivity was measured during the crystallization process of CaCO_3 in water at 45 °C, from 0 to 1500 s. This was achieved by using CaCl_2 (0.04 mol/L, 50 mL) and Na_2CO_3 (0.04 mol/L, 50 mL). Additionally, HABS (24 mg) and kerosene (20 mL) were added in situ to the above solution through stirring at 1000 rpm, resulting in the formation of a HABS-controlled kerosene emulsion. The electrical conductivity was continuously monitored from 1500 to 3840 s to investigate the dissolution and transformation of CaCO_3 in emulsion.

To investigate the influence of HABS on the precipitation process and the dissolution process, respectively, zeta potential and pH were measured every 5 min in both water and HABS (200 mg/L)-controlled O/W emulsion at 45 °C.

2.3. Characterization

The morphology of the obtained samples was characterized using a scanning electron microscope (SEM, Zeiss SIGMA, Oberkochen, Germany) with an acceleration voltage of 10 kV. Elemental analysis was carried out using an energy dispersive X-ray analyzer (EDX), which was directly connected with the SEM at an accelerating voltage of 20 kV. Fourier transform infrared (FT-IR) spectra were measured using KBr pellets on a Tensor27 spectrometer (Ettlingen, Germany). Powder X-ray diffraction (pXRD) patterns were measured using a D/max 2200PC diffractometer (Rigaku, Tokyo, Japan) fitted with $\text{Cu-K}\alpha$ ($\lambda = 1.54 \text{ \AA}$) radiation at 40 kV and 20 mA, employing a step size of $10^\circ/\text{min}$ with 2θ ranging from 10° to 80° . Transmission electron microscope (TEM) observations were recorded (Tecnail G2S-Twin F20) at an accelerating voltage of 200 kV, and all samples were prepared via the deposition of ethanol dispersions on carbon films supported by a copper grid for HRTEM measurements (Hillsboro, USA). The electrical conductivity (EC) data were recorded using a DDS-11A electrical conductivity meter (Shanghai, China). The zeta potential was determined at 45 °C (Malvern Nano ZS, Worcestershire, UK). The water contact angle of CaCO_3 crystals was determined using a contact angle meter (KRÜSS DSA30, Hamburg, Germany), which describes the surface characteristic of particles and the variation with different HABS concentrations. A CaCO_3 tablet was pressed in the sample presser. A drop of water was added to the CaCO_3 tablet's surface to measure the contact angle.

2.4. Calculation Method of Relative Fraction of Aragonite, Vaterite and Calcite

The relative mole fractions of vaterite, aragonite and calcite were calculated from their characteristic pXRD peak intensities using the following equations [25]:

$$X_V = 7.691 \frac{I_V^{110}}{I_C^{104} + 7.691(I_V^{110}) + 3.157(I_A^{221})} \quad (1)$$

$$X_V + X_A + X_C = 1 \quad (2)$$

$$\frac{I_C^{104}}{I_V^{110}} = 7.691 \frac{X_C}{X_V} \quad (3)$$

$$X_V + X_C = 1 \quad (4)$$

$$\frac{I_C^{104}}{I_A^{221}} = 3.157 \frac{X_C}{X_A} \quad (5)$$

$$X_A + X_C = 1 \quad (6)$$

where X_A is the mole fraction of aragonite, X_V is the mole fraction of vaterite and X_C is the mole fraction calcite. I_C^{104} , I_A^{221} and I_V^{110} are the pXRD intensities of the {104} planes, {221} planes and {110} planes, representing calcite, aragonite and vaterite, respectively.

3. Results and Discussion

A simulated mineralization approach was designed by mixing HABS/Na₂CO₃ solution and CaCl₂/kerosene emulsion (20 V% O/W) to prepare the mixed aragonite crystals. As can be seen in Figure 1, CaCO₃ crystals present bouquet-like and dumbbell-like morphologies with radiated bundles. A key question is how crystals of vaterite–aragonite, aragonite and calcite–aragonite can be molded into such convoluted morphologies. Aiming to study the crystallization process of CaCO₃ in a HABS-controlled kerosene emulsion system, a series of CaCO₃ precipitates were synthesized by changing the concentration of HABS, reaction temperature and time (Tables S1–S3). As a result, rosette-like, bouquet-like, and dumbbell-shaped CaCO₃ crystals with vaterite–aragonite, aragonite, and calcite–aragonite phases were formed with a 200 mg/L HABS concentration at 45 °C for 60 min. The spherical vaterite phase can be stabilized at a high HABS concentration (800 mg/L and 1000 mg/L). Rhombohedral calcite content experienced a fluctuation of about 40% as the HABS concentration varied. Needle-like and bundle-like aragonites are generated with increasing temperatures from 65 °C to 85 °C.

3.1. Effects of HABS on the Polymorphic CaCO₃ Crystals

Aiming to investigate the effect of HABS concentration on the polymorph and morphology of CaCO₃ products in kerosene emulsions, experiments were carried out at 45 °C for 1 h with different HABS concentrations. Simultaneously, the corresponding CaCO₃ crystals were characterized by SEM, FTIR and pXRD. Figure 2 shows the morphological evolution of CaCO₃ under different HABS concentrations. It is observed that rosette-like, dumbbell-shaped, spherical and rhombohedral crystals were obtained with a wide size distribution from 5 to 10 μm at lower HABS concentrations (200 mg/L, 400 mg/L, 600 mg/L), especially at 200 mg/L. And, the calculated relative amounts of rosette-like, dumbbell-shaped aragonite were 29.70%, 10.07%, and 12.27%, respectively; those of spherical vaterite were 39.73%, 44.22%, and 53.72%; and those of rhombohedral calcite were 30.57%, 40.71%, and 34.01% (Table S1). Increasing the HABS concentration to 800 mg/L and 1000 mg/L, spherical vaterite was more prominent. We can speculate that vaterite nuclei form on the HABS surfaces due to a reduction in the activation energy of nucleation (ΔG) through interfacial recognition, thus making kinetic control of vaterite possible [26].

On this basis, the increasing interaction of sulfonate groups of HABS and Ca^{2+} could gradually induce the formation of less-stable vaterite crystals. These spherical structures aggregated with many nano-sized particles, showing rough surfaces (Figure S1). It is likely that these vaterite particles were initially formed by the aggregation of amorphous calcium carbonate nanoparticles, and upon their transformation into crystalline vaterite, vaterite then transformed to calcite via a “dissolution-precipitation mechanism” [27].

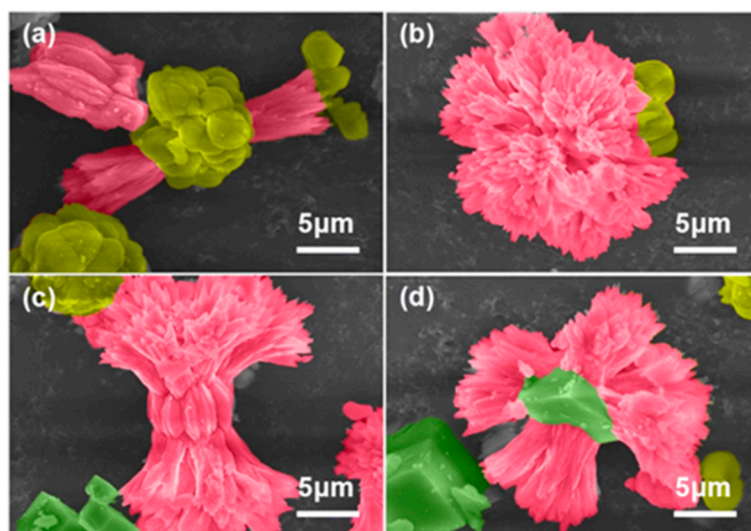


Figure 1. SEM images of CaCO_3 crystals in HABS-controlled kerosene emulsion. Yellow colors, green colors and pink colors represent vaterite, calcite, and aragonite, respectively. (a) bouquet-like vaterite–arononite, (b) rosette-like vaterite–arononite, (c) dumbbell-like aragonite, (d) calcite–arononite.

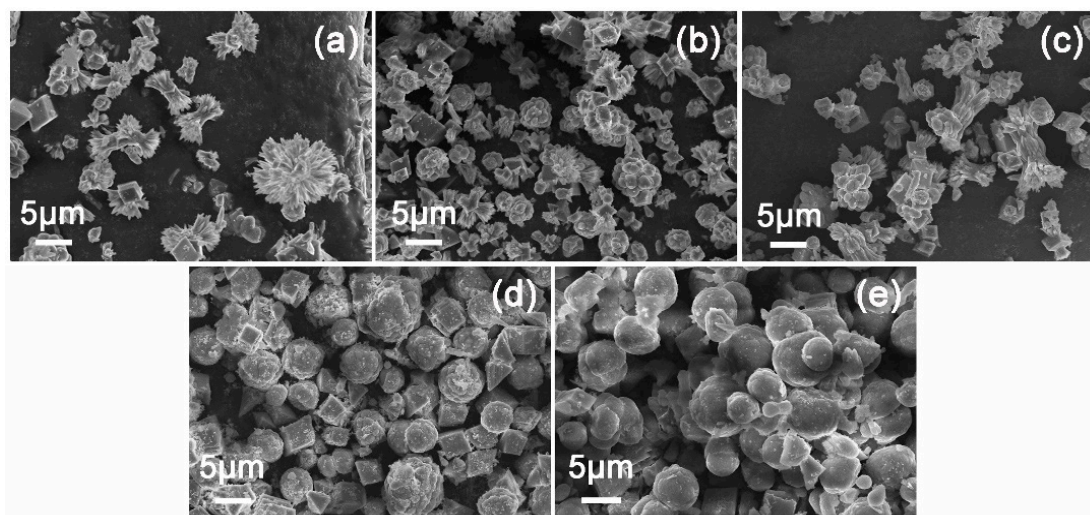


Figure 2. Morphologies of CaCO_3 under various HABS concentration ((a): 200 mg/L; (b): 400 mg/L; (c): 600 mg/L; (d): 800 mg/L; (e): 1000 mg/L).

Generally, there are four main FTIR adsorption bands of C-O bond vibrations with regard to CaCO_3 , including symmetric stretching (ν_1), out-of-plane bending (ν_2), asymmetric stretching (ν_3) and in-plane bending (ν_4) [28,29]. According to the FTIR results (Figure 3a), three characteristic peaks were found at 1471 cm^{-1} , $876/856\text{ cm}^{-1}$ and $745/713\text{ cm}^{-1}$ in the lower concentrations (200 mg/L, 400 mg/L, 600 mg/L), indicating that these precipitates were the mixed phase of calcite, aragonite and vaterite [30]. With the increase in the HABS concentration, the tendency to form vaterite increased, indicating a strong stabilization of the vaterite phase by high HABS concentrations (800 mg/L and 1000 mg/L). Especially when the HABS concentration was greater than 800 mg/L, a mixture of vaterite and calcite

(875 cm^{-1} , $745/713\text{ cm}^{-1}$) was obtained, without aragonite being found. In addition, the obtained CaCO_3 had specific peaks around 3500 cm^{-1} , $2800\text{--}3000\text{ cm}^{-1}$, 1400 cm^{-1} and 1045 cm^{-1} , which corresponded to the stretching vibration of $-\text{OH}$, the alkyl chain, $\text{S}=\text{O}$, and $\text{S}-\text{O}$ in HABS, respectively (Figure 3a). Precipitates also presented an increase in water contact angle from 4.4° to 75.3° , with the increases in HABS concentrations from 200 mg/L to 600 mg/L , suggesting a change in the CaCO_3 surface from hydrophilic to hydrophobic properties (Figure 3b). Also, the water contact angle increased slightly to 82.5° at 1000 mg/L HABS. The upward trend was different with the lower HABS concentrations, which might be due to the decreases in the amount of specific polymorphs of CaCO_3 . Thus, the surface activity of CaCO_3 particles can be enhanced by the adsorption of hydrophobic alkyl chains in HABS, which are electrostatically attached to the surface of the CaCO_3 particles, resulting in a higher water contact angle [31,32].

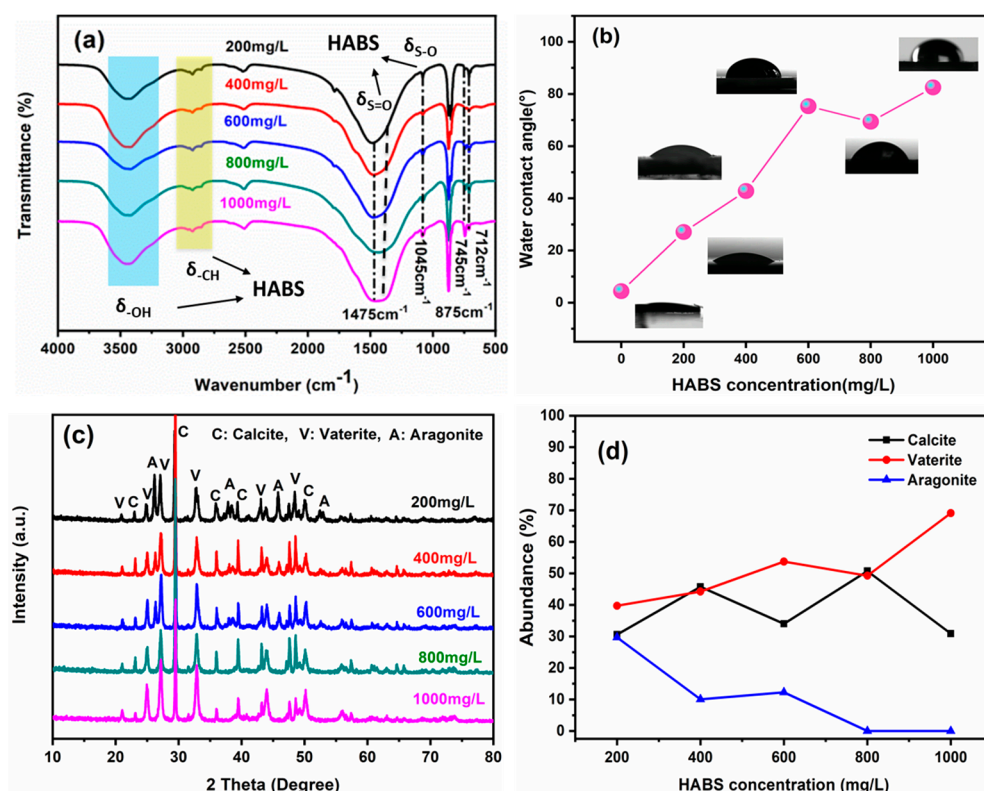


Figure 3. FTIR (a), water contact angle (b), XRD (c), and CaCO_3 crystal content (d) under various HABS concentrations.

The pXRD analysis of the prepared particles was also performed to gain information on the structural changes of those products, revealing that they underwent a polymorph evolution process. Precisely, the pXRD patterns of solids formed at the lower HABS concentrations (200 mg/L , 400 mg/L , 600 mg/L), shown in Figure 3c, show Bragg peaks at (2θ) 29.4° , 24.9° , 27° , 32.8° , 36.2° and 41.2° that can be assigned to the (104), (110), (112), (114), (220) and (221) crystalline planes of calcite, vaterite and aragonite, respectively [33]. When the HABS concentration increased to 800 mg/L and 1000 mg/L , the reflections of aragonite disappeared, and vaterite became dominant. Importantly, the polymorphs of these samples are consistent with FTIR patterns. Calculations of polymorphic ratios and the content of vaterite, calcite and aragonite are shown in Figure 3c,d [34]. Notably, calcite content experienced a fluctuation of about 40% as the HABS concentration varied. With the increase in the HABS concentration, the tendency to form aragonite declined from 30% at 200 mg/L to 0 at 800 mg/L . Interestingly, the content of vaterite progressively dominated, indicating that the higher HABS concentration ($>800\text{ mg/L}$) exerted a strong

stabilization effect on vaterite due to their influence on ion migration, accumulation and oriented deposition [10].

3.2. Effects of Reaction Time and Temperature on the Polymorphic CaCO_3 Crystals

To further investigate the growth mechanism, time-resolved experiments were performed in a 600 mg/L HABS solution at 45 °C. Figure 4 shows the SEM images of the temporal evolution of the CaCO_3 products generated. During the first 20 min of the crystallization process, many highly aggregated particles with several micrometers of CaCO_3 emerged (Figure 4a–c). The coalescence behavior of the rounded crystals indicates that in the initial stage, HABS is stable at the oil–water interface, attracting negatively charged CaCO_3 via electrostatic attraction (Figure S2). It is speculated that the presence of ACC on the oil/water interface promoted the stability of oil droplets, as in a Pickering emulsion, thus leading to the formation of larger particles during the growth stage, as previously reported [10,33,35]. Branching needles and rhombohedral bulks were obtained after 30 min of crystallization, indicating that the transformation from vaterite to metastable aragonite and stable calcite was in progress (Figures 4d and S3). After 60 min of crystallization, particles with cauliflower-shaped spherical aggregates, bouquet-like and dumbbell-like needles, and rhombohedral bulks can be observed (Figure 4e).

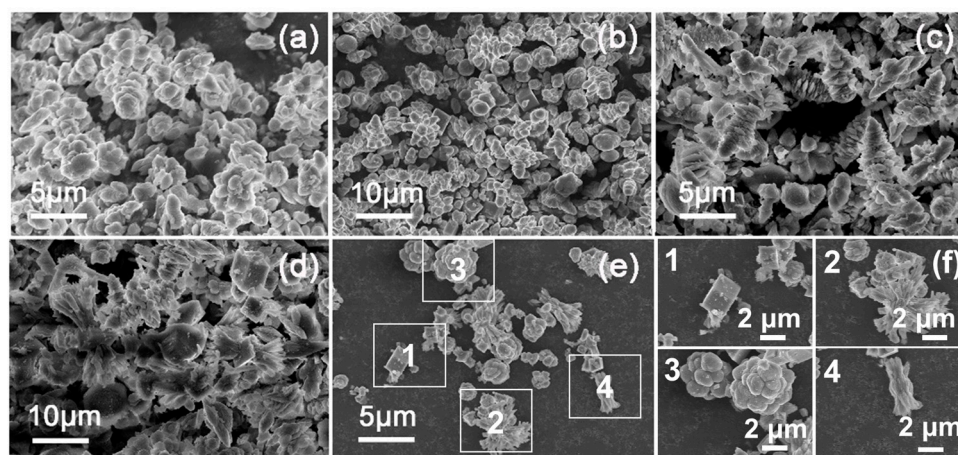


Figure 4. SEM images of CaCO_3 crystals in kerosene emulsion with various reaction times: (a) 5 min, (b) 10 min, (c) 20 min, (d) 30 min, (e) 60 min and (f) enlarged view of (e). And (1) presents rhombohedral calcite, (2) bouquet-like calcite-aragonite, (3) cauliflower-shaped vaterite, and (4) dumbbell-like aragonite.

To gain insight into the influence of reaction temperature on the crystallization of CaCO_3 in this unique system, the morphological changes in the precipitated particles as a function of temperature were studied with SEM, as shown in Figure 5. Specifically, when the reaction temperature was 35 °C, the particles were sphere-aggregated with a diameter of about 6 μm (Figure 5a), whereas when the reaction temperature increased to 45 °C, the precipitated particles were in rhombohedral-like, dumbbell-shaped and sphere-aggregated forms with irregular size (Figure 5b). At 55 °C, a large number of disordered products were formed (Figure 5c). The morphologies of these particles became needle-like and bundle-like (Figure 5d–f) with increasing temperature (65 °C, 75 °C, and 85 °C). Moreover, a mixture of vaterite and calcite was obtained at 35 °C, and as the reaction temperature increased above 45 °C, the aragonite phase emerged. The XRD spectra of various CaCO_3 samples corroborated the FTIR results. The fraction of aragonite increased progressively from 5% to 70% as the reaction temperature was increased from 45 °C to 85 °C, and the proportion of calcite decreased from 50% to 10% (Figure S4).

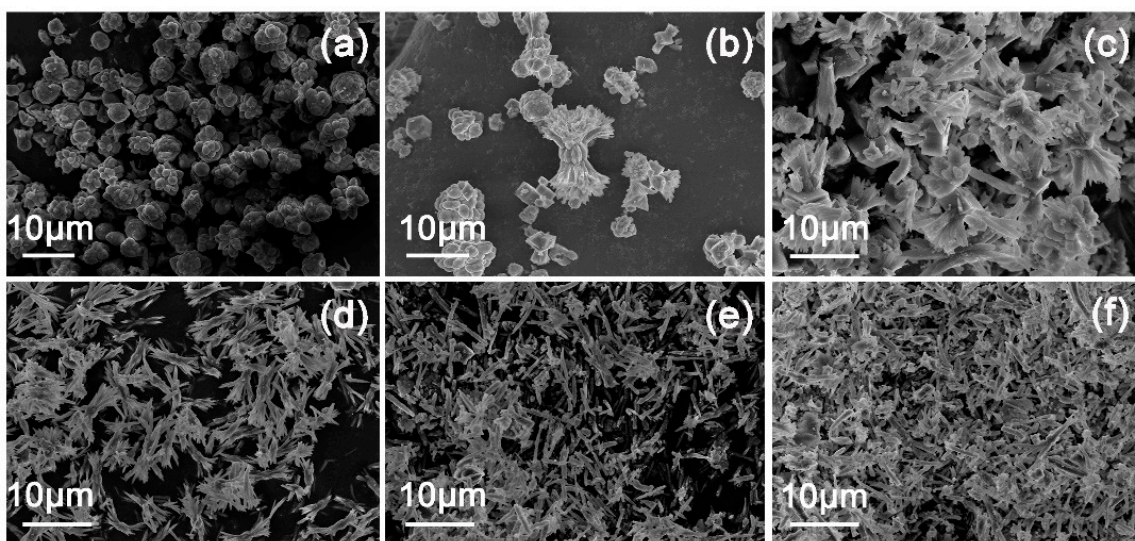


Figure 5. SEM images of CaCO_3 crystals in kerosene emulsion with various reaction temperatures (a–f): 35 °C, 45 °C, 55 °C, 65 °C, 75 °C and 85 °C.

3.3. Possible Growth Model of the Polymorphic Mixed CaCO_3 Crystals

The mineralization of CaCO_3 under general conditions tends to form metastable ACC first and then transform to crystalline phase vaterite, aragonite and calcite [36]. On the basis of the above-mentioned investigations, the formation of CaCO_3 can be identified in four steps: the mixing of CO_3^{2-} and HABS molecules; the pre-nucleation stage (containing the formation of ion pairs and pre-nucleation clusters); the nucleation stage; and the post-nucleation stage (crystallization of vaterite, aragonite and calcite) [37,38]. Generally, calcite is a kind of high-pressure, stable-phase mineral. Aragonite will naturally transform into calcite. However, in the presence of a strong driving force (which is affected by the HABS concentration and temperature of the substance), calcite may be dissolved and result in the nucleation of ACC, which in turn can transform into vaterite or aragonite.

A schematic model of the possible growth of CaCO_3 crystals in the HABS/kerosene emulsion is shown in Figure 6. Generally, CaCO_3 crystallization involves a transformation from ACC to vaterite, then undergoing a vaterite–calcite transformation or a vaterite–aragonite transformation under higher temperature conditions (Figure 6a) [27,39]. In general, micelles will appear when HABS exists in aqueous solution [10]. Due to the high surface energy of micelles, calcium ions and carbonate ions in solution will be adsorbed to the surface of micelles, thus promoting the aggregation of ions. When there is an appropriate amount of amorphous CaCO_3 on the micellar surface undergoing the vaterite formation process, the increase in temperature leads to the formation of aragonite. Additionally, HABS and the emulsion alter the surface or interface of calcite, serving as nucleation sites. In the presence of an excess of amorphous CaCO_3 , vaterite and aragonite undergo heterogeneous nucleation on calcite [40]. The synergistic effect of HABS and temperature can regulate the transformation from vaterite to aragonite (Figure 6c). Thus, aragonite-based polymorphic mixed CaCO_3 crystals are obtained at 45 °C with the help of HABS and a small quantity of kerosene matrix.

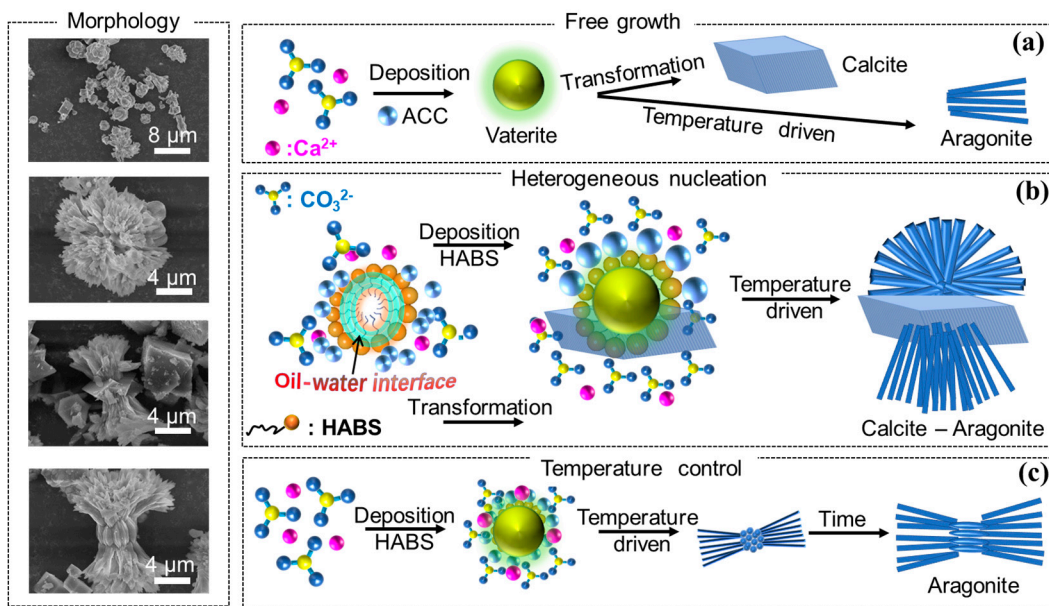


Figure 6. Schematic models of the possible growth of CaCO_3 crystals in HABS/kerosene emulsion. (a) In general, the crystallization and transformation of CaCO_3 . (b) vaterite and aragonite undergo heterogeneous nucleation on calcite, (c) the transformation from vaterite to aragonite.

In addition, the dissolution of CaCO_3 minerals in the ocean is a fundamental part of marine alkalinity. The freshwater dissolution rate of calcite has been well described, with the determining factors affecting the dissolution of calcite including temperature, pressure, ionic strength, pH, zeta potential, and the degree of saturation of solution relative to calcite [41,42]. To further investigate calcite dissolution and the transformation of ACC to vaterite and aragonite during this crystallization process, the electrical conductivity was performed together with pH, XRD, SEM, EDS and TEM characterizations (Figures 7 and S6).

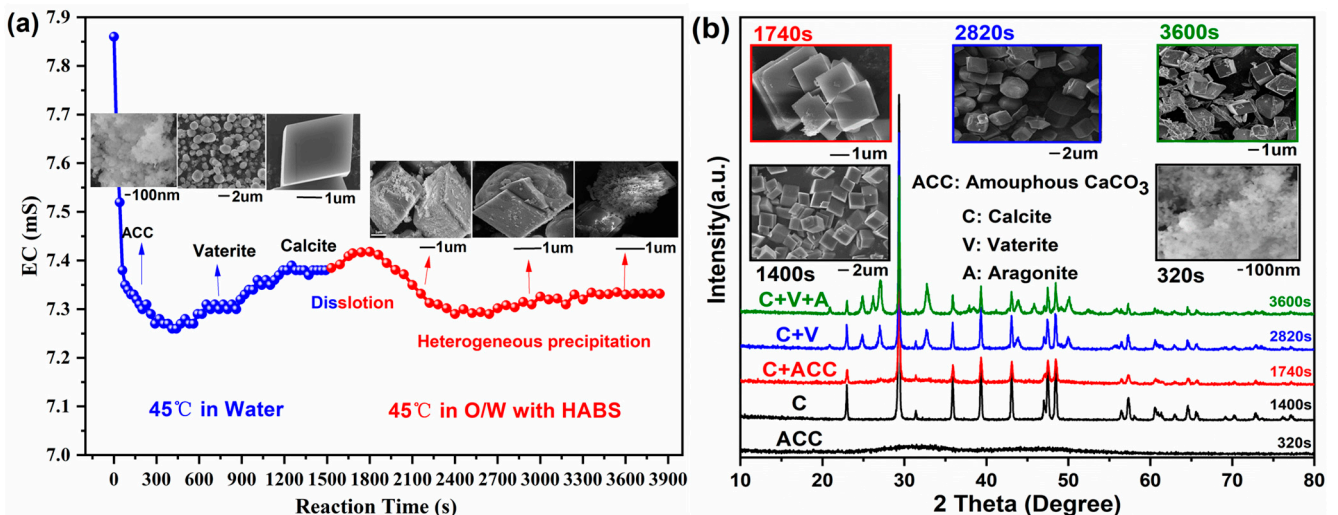


Figure 7. Electrical conductivity of pure calcite, calcite dissolution and precipitation in O/W with HABS (a), and their correlative XRD patterns and SEM images (b).

In Figure 7a, the electrical conductivity value decreased at a rapid rate due to the consumption of Ca^{2+} and CO_3^{2-} in the initial CaCO_3 precipitation process and reached a minimum upon completion of the precipitation process. The EC decreased quickly within 450 s, and there were only Ca^{2+} , Cl^- , CO_3^{2-} , and Na^+ in the solution. Among the

above ions, the maximum nucleation rate occurred in solutions with initial stoichiometric $\text{Ca}^{2+}/\text{CO}_3^{2-}$ concentrations due to the K_{sp} of CaCO_3 being the lowest. Thus, the EC decreased quickly in the first 5 min. Then, the electrical conductivity increased via a low ebb valley, where the transformation of ACC to vaterite was due to an internal structural reorganization within the individual nanoparticles, which occurred from 450 s to 900 s. The transformation of vaterite to calcite was from 900 s to 1200 s. Finally, pure calcite was generated with the electrical conductivity reaching a certain value (as seen in the blue circles in Figure 7a).

Immediately after, HABS (24 mg) and kerosene (20 mL) were added in situ to the above solution through stirring at 1000 rpm, resulting in the formation of a HABS-controlled kerosene emulsion. The electrical conductivity was continuously monitored from 1500 to 3840 s to investigate the processes of dissolution and transformation of CaCO_3 in emulsion. The EC increased from 1520 s to 2400 s, owing to the dissolution of a portion of calcite, where the Ca^{2+} and CO_3^{2-} formed (as seen in the red circle in Figure 7a). Figure S5 showed that the dissolution of calcite occurred from rhombic cross-sections (the terrace between two steps) and diffused toward a step edge, creeping along it, to reach the kink site [43]. Then, the ACC particles generated via the consumption of Ca^{2+} and CO_3^{2-} (two broad humps between 25° and 55° in XRD and SEM of 1740 s in Figure 7b, no lattice fringe HRTEM image in Figure S6e, and EDX in Figure S6f). ACC transformed to vaterite and aragonite from 2700 s to 3360 s with an increase in EC. Finally, once the electrical conductivity reached a certain value, the mixed crystals of calcite, vaterite and aragonite were obtained (XRD and SEM images of 2820 s and 3600 s in Figure 7).

In addition, zeta potential and pH were measured to investigate the influence of HABS on the precipitation process and the dissolution process, respectively. During the process of CaCO_3 crystallization, the potential in the HABS system was higher than that in pure water. The hydrolysis and ionization of HABS produce a large amount of negative charges, which combine with calcium carbonate, resulting in an increase in negative charges on their surfaces. The increase in the surface charge leads to more stable CaCO_3 aqueous dispersions and is attributed to the distribution of the calcium/sulfonate ions pairs on the solid surface, which is fully consistent with Lim' results: the adsorption of HABS molecules on CaCO_3 particles is driven not only by the electrostatic interaction but also by the hydrophobic effect (Figure S7a) [32]. Also, pH results indicate that the transformation of ACC to calcite is prevented and the thermodynamically unstable vaterite is intercepted with the help of HABS (Figure S7b).

During the process of calcium carbonate dissolution, the potential in the HABS system was also higher than that in pure water (Figure S7c). Larsen reported that the weakly bonded Ca^{2+} on the energetics of calcite surface sites will dissolve due to the thermal motion and electrostatic attraction of molecules in solution, leading to kinks on the crystal edges (Figure 7b) [43]. Meanwhile, the pH decreased as time increased, proving that the migration ability of CO_3^{2-} is better than Ca^{2+} (Figure S7d). Mahrouqi concluded that when the pH and potential are in equilibrium, CaCO_3 will also reach dissolution and deposition equilibrium [44]. HABS alter the surface property of calcite, leading to a HABS–solid phase interaction, which can greatly influence the CaCO_3 particle's stability, ion aggregation behavior, and phase transformation. Thus, a portion of calcite can undergo dissolution into ions, which in turn can combine leading to ACC precipitation, then forming aragonite-based polymorphic mixed CaCO_3 crystals.

4. Conclusions

In summary, aragonite-based mixed CaCO_3 crystals with superstructures were obtained in a HABS/kerosene O/W emulsion. It was found that HABS has a stabilizing effect on metastable CaCO_3 phases and on the interface between kerosene and water. There is a synergistic effect between HABS and the temperature in kerosene emulsion, which assists the formation of CaCO_3 with special morphologies, such as rosette-like, bouquet-like and dumbbell-like superstructures. This work explained how an anionic surfactant such as HABS

regulates the crystallization of CaCO₃ systemically in O/W emulsion systems. This work is also important for understanding the formation of minerals in natural environments and in the development of materials with specific properties. It may also have implications for the design of biomimetic materials that mimic the mineralization processes found in nature.

Supplementary Materials: The following supporting information can be downloaded at: <https://www.mdpi.com/article/10.3390/cryst13071107/s1>, Figure S1: SEM images of vaterite particles and the corresponding enlarged view; Figure S2: Images of ACC migration. Left: water, Right: HABS/kerosene /water; Figure S3: FTIR, XRD and content variation of CaCO₃ at 45 °C under various reaction times (5 mins, 10 mins, 20 mins, 30 mins, and 60 mins); Figure S4. FTIR, XRD and content variation of CaCO₃ under reaction temperature(35 °C, 45 °C, 55 °C, 65 °C, 75 °C, and 85 °C); Figure S5: SEM images collected during the calcite dissolution process from 1500s to 2400s; Figure S6: SEM images at reaction time of 1400s (a) and 2820s (b); Figure S7: Trends in pH and Zeta potential during calcite precipitation process and calcite dissolution process in different systems. TEM, HRTEM, and EDS of the typical mixed crystal, respectively (c)–(f); Table S1: Fraction of vaterite, aragonite and calcite in kerosene emulsions with various concentrations of HABS; Table S2: Fraction of vaterite, aragonite and calcite in kerosene emulsions with various reaction times; Table S3: Fraction of vaterite, aragonite and calcite in kerosene emulsions with various reaction temperatures.

Author Contributions: Conceptualization, methodology, investigation, writing—original draft, W.H.; formal analysis, data curation, investigation, J.H., W.S. (Weihaio Sun), J.L. and H.G.; methodology, resources, validation, C.Z., Q.W., X.L. and M.C.; conceptualization, funding acquisition, project administration, supervision, writing—review and editing, W.S. (Weiguang Shi) All authors have read and agreed to the published version of the manuscript.

Funding: This work was financial supported by the National Natural Science Foundation of China (#51404069) and the State Key Laboratory Opening Project Foundation of Jilin University (#2018-16).

Data Availability Statement: Data can be made available upon request from the corresponding author.

Acknowledgments: We are grateful to the group of Xiaoyang Liu (State Key Laboratory of Inorganic Synthesis and Preparative Chemistry, College of Chemistry, Jilin University) and the microscopic test center of the Northeast Petroleum University for characterization.

Conflicts of Interest: The authors declare no conflict of interest.

Abbreviations

HABS: heavy alkyl-benzene sulfonate; ASP: alkaline/surfactant/polymer flooding; ACC: amorphous calcium carbonate; HPAM: partially hydrolyzed polyacrylamide.

References

1. Liu, Z.; Shao, C.; Jin, B.; Zhang, Z.; Zhao, Y.; Xu, X.; Tang, R. Crosslinking ionic oligomers as conformable precursors to calcium carbonate. *Nature* **2019**, *574*, 394–398. [[CrossRef](#)] [[PubMed](#)]
2. Zhang, A.; Xiao, Z.; Liu, Q.; Li, P.; Xu, F.; Liu, J.; Tao, H.; Feng, L.; Song, S.; Liu, Z.; et al. CaCO₃-Encapsulated Microspheres for Enhanced Transhepatic Arterial Embolization Treatment of Hepatocellular Carcinoma. *Adv. Healthc. Mater.* **2021**, *10*, 2100748. [[CrossRef](#)] [[PubMed](#)]
3. Feng, Z.; Yang, T.; Liang, T.; Wu, Z.; Wu, T.; Zhang, J.; Yu, L. Biomineralization of calcium carbonate under amino acid carbon dots and its application in bioimaging. *Mater. Des.* **2022**, *217*, 110644. [[CrossRef](#)]
4. Liu, Z.; Zhang, Z.; Wang, Z.; Jin, B.; Li, D.; Tao, J.; Tang, R.; De Yoreo, J.J. Shape-preserving amorphous-to-crystalline transformation of CaCO₃ revealed by in situ TEM. *Proc. Natl. Acad. Sci. USA* **2020**, *117*, 3397–3404. [[CrossRef](#)]
5. Politi, Y.; Arad, T.; Klein, E.; Weiner, S.; Addadi, L. Sea Urchin Spine Calcite Forms via a Transient Amorphous Calcium Carbonate Phase. *Science* **2004**, *306*, 1161–1164. [[CrossRef](#)]
6. Liu, R.; Liu, F.; Zhao, S.; Su, Y.; Wang, D.; Shen, Q. Crystallization and oriented attachment of monohydrocalcite and its crystalline phase transformatio. *CrystEngComm* **2013**, *15*, 509–515. [[CrossRef](#)]
7. Rodríguez-Ruiz, I.; Veessler, S.; Goómez-Morales, J.; Delgado-Lopez, J.M.; Grauby, O.; Hammadi, Z.; Candoni, N.; García-Ruiz, J.M. Transient Calcium Carbonate Hexahydrate (Ikaite) Nucleated and Stabilized in Confined Nano- and Picovolumes. *Cryst. Growth Des.* **2014**, *14*, 792–802. [[CrossRef](#)]

8. Liu, X.; Wang, Y.; Ma, Z.; Zhou, W.; Wang, X.; Zhou, H.; Wang, X.; Wang, J.; Shi, W. HABS-Silicate Controlled Synthesis of Worm-Like Calcite via Orientated Attachment. *ChemistrySelect* **2021**, *6*, 1199–1203. [[CrossRef](#)]
9. Pokroy, B.; Zolotoyabko, E. Aragonite growth on single-crystal substrates displaying a threefold axis. *Chem. Commun.* **2005**, *16*, 2140–2142. [[CrossRef](#)]
10. Shi, W.; Ma, Z.; Mu, Y.; Wang, J.; Liu, X.; Dong, Z.; Wang, S.; Bai, M.; Teng, Z. Interfacial self-propagation of oleophilic vaterite in crude oil emulsion and its application for reinforcing polyethylene. *Powder Technol.* **2020**, *363*, 642–651. [[CrossRef](#)]
11. Zou, Z.; Habraken, W.J.E.M.; Matveeva, G.; Jensen, A.C.S.; Bertinetti, L.; Hood, M.A.; Sun, C.; Gilbert, P.U.P.A.; Polishchuk, I.; Pokroy, B.; et al. A hydrated crystalline calcium carbonate phase: Calcium carbonate hemihydrate. *Science* **2019**, *363*, 396–400. [[CrossRef](#)] [[PubMed](#)]
12. Li, Y.-X.; Jiang, Y. Synergistic Occlusion of Doxorubicin and Hydrogels in CaCO₃ Composites for Controlled Drug Release. *Crystals* **2023**, *13*, 132. [[CrossRef](#)]
13. Ueno, Y.; Futagawa, H.; Takagi, Y.; Ueno, A.; Mizushima, Y. Drug-incorporating calcium carbonate nanoparticles for a new delivery system. *J. Control. Release* **2005**, *103*, 93–98. [[CrossRef](#)]
14. Sheng, K.; Ge, H.; Huang, X.; Zhang, Y.; Song, Y.; Ge, F.; Zhao, Y.; Meng, X. Formation and inhibition of calcium carbonate crystals under cathodic polarization conditions. *Crystals* **2020**, *10*, 275. [[CrossRef](#)]
15. Balthasar, U.; Cusack, M. Aragonite-calcite seas—Quantifying the gray area. *Geology* **2015**, *43*, 99–102. [[CrossRef](#)]
16. Robles-Fernández, A.; Areias, C.; Daffonchio, D.; Vahrenkamp, V.C.; Sánchez-Román, M. The role of microorganisms in the nucleation of carbonates, environmental implications and applications. *Minerals* **2022**, *12*, 1562. [[CrossRef](#)]
17. Li, M.; Lebeau, B.; Mann, S. Synthesis of Aragonite Nanofilament Networks by Mesoscale Self-Assembly and Transformation in Reverse Microemulsions. *Adv. Mater.* **2003**, *15*, 2032–2035. [[CrossRef](#)]
18. Zhou, G.T.; Yao, Q.Z.; Ni, J.; Jin, G. Formation of aragonite mesocrystals and implication for biomineralization. *Am. Mineral.* **2009**, *94*, 293–302. [[CrossRef](#)]
19. Fermani, S.; Džakula, B.N.; Reggi, M.; Falini, G.; Kralj, D. Effects of magnesium and temperature control on aragonite crystal aggregation and morphology. *CrystEngComm* **2017**, *19*, 2451–2455. [[CrossRef](#)]
20. Yang, L.; Chu, D.; Sun, H.; Ge, G. Room temperature synthesis of flower-like CaCO₃ architectures. *New J. Chem.* **2016**, *40*, 571–577. [[CrossRef](#)]
21. Cheng, J.; Zhou, W.; Wang, Q.; Cheng, T.; Zhou, G. Morphology and crystallization character of calcium carbonate in scaled sample formed during alkaline surfactant-polymer (ASP) flooding in Daqing Oilfield. *Chem. J. Chin. Univ.* **2012**, *33*, 1138–1142.
22. Jing, G.; Tang, S.; Yu, T.; Gai, Y. Effect of HPAM in ASP flooding wastewater on scaling. *Desalination Water Treat.* **2014**, *52*, 6930–6935. [[CrossRef](#)]
23. Jing, G.; Tang, S.; Li, X. Effect of HPAM on calcium carbonate crystallization. *J. Korean Chem. Soc.* **2013**, *57*, 365–369. [[CrossRef](#)]
24. Ma, Z.; Mu, Y.; Shi, W.; Wang, J.; Liu, X.; Wang, X.; Dong, Z. HPAM–HABS induced synthesis of a labyrinth-like surface of calcite via rhombohedral lattice growth from the nanoscale. *CrystEngComm* **2018**, *20*, 3445–3448. [[CrossRef](#)]
25. Lai, Y.; Chen, L.; Bao, W. Glycine-mediated, selective preparation of monodisperse spherical vaterite calcium carbonate in various reaction systems. *Cryst. Growth Des.* **2015**, *15*, 1194–1200. [[CrossRef](#)]
26. Park, H.K.; Lee, I.; Kim, K. Controlled growth of calcium carbonate by poly(ethylenimine) at the air/water interface. *Chem. Commun.* **2004**, *1*, 24–25. [[CrossRef](#)] [[PubMed](#)]
27. Rodriguez-Blanco, J.D.; Shaw, S.; Benning, L.G. The kinetics and mechanisms of amorphous calcium carbonate (ACC) crystallization to calcite, via vaterite. *Nanoscale* **2011**, *3*, 265–271. [[CrossRef](#)] [[PubMed](#)]
28. Zheng, L.; Hu, Y.; Ma, Y.; Zhou, Y.; Nie, F.; Liu, X.; Pei, C. Egg-white-mediated crystallization of calcium carbonate. *J. Cryst. Growth* **2012**, *361*, 217–224. [[CrossRef](#)]
29. Guo, B.; Zhao, T.; Sha, F.; Zhang, F.; Li, Q.; Zhang, J. Control over crystallization of CaCO₃ micro-particles by a novel CO₂SM. *CrystEngComm* **2015**, *17*, 7896–7904. [[CrossRef](#)]
30. Shi, W.; Ma, Z.; Wang, Y.; Wang, J.; Li, B.; Wang, X.; Zhou, W.; Cheng, J. HPAM assisted controllable synthesis of peanut-like CaCO₃ in fixed silicate solution. *Colloids Surf. A* **2017**, *535*, 34–40. [[CrossRef](#)]
31. Cui, Z.G.; Cui, Y.Z.; Cui, C.F.; Chen, Z.; Binks, B.P. Aqueous foams stabilized by in situ surface activation of CaCO₃ nanoparticles via adsorption of anionic surfactant. *Langmuir* **2010**, *26*, 12567–12574. [[CrossRef](#)] [[PubMed](#)]
32. Song, E.; Kim, D.; Kim, B.J.; Lim, J. Surface modification of CaCO₃ nanoparticles by alkylbenzene sulfonic acid surfactant. *Colloids Surf. A* **2014**, *461*, 1–10. [[CrossRef](#)]
33. Dai, Y.; Zou, H.; Zhu, H.; Zhou, X.; Song, Y.; Shi, Z.; Sheng, Y. Controlled synthesis of calcite/vaterite/aragonite and their applications as red phosphors doped with Eu³⁺ ions. *CrystEngComm* **2017**, *19*, 2758–2767. [[CrossRef](#)]
34. Sarkar, A.; Dutta, K.; Mahapatra, S. Polymorph Control of Calcium Carbonate Using Insoluble Layered Double Hydroxide. *Cryst. Growth Des.* **2013**, *13*, 204–211. [[CrossRef](#)]
35. Zhu, Y.; Chen, T.; Cui, Z. Multiple Pickering emulsions stabilized by the same particles with different extent of hydrophobization in situ. *Front. Chem.* **2022**, *10*, 950932. [[CrossRef](#)]
36. Porras, M.; Solans, C.; González, C.; Gutiérrez, J.M. Properties of water-in-oil (W/O) nano-emulsions prepared by a low-energy emulsification method. *Colloids Surf. A* **2008**, *324*, 181–188. [[CrossRef](#)]
37. Bots, P.; Benning, L.G.; Rodriguez-Blanco, J.D.; Roncal-Herrero, T.; Shaw, S. Mechanistic Insights into the Crystallization of Amorphous Calcium Carbonate (ACC). *Cryst. Growth Des.* **2012**, *12*, 3806–3814. [[CrossRef](#)]

38. Farhadi-Khouzani, M.; Chevrier, D.M.; Zhang, P.; Hedin, N.; Gebauer, D. Water as the key to proto-aragonite amorphous CaCO₃. *Angew. Chem. Int. Ed.* **2016**, *55*, 8117–8120. [[CrossRef](#)]
39. Radha, A.V.; Forbes, T.Z.; Killian, C.E.; Gilbert, P.U.P.A.; Navrotsky, A. Transformation and crystallization energetics of synthetic and biogenic amorphous calcium carbonate. *Proc. Natl. Acad. Sci. USA* **2010**, *107*, 16438–16443. [[CrossRef](#)]
40. Goöppert, A.K.; Gonzalez-Rubio, G.; Schnitzlein, S.; Coölfen, H. A nanoparticle-based model system for the study of heterogeneous nucleation phenomena. *Langmuir* **2023**, *39*, 3580–3588. [[CrossRef](#)]
41. Adkins, J.F.; Naviaux, J.D.; Subhas, A.V.; Dong, S.; Berelson, W.M. The dissolution rate of CaCO₃ in the ocean. *Annu. Rev. Mar. Sci.* **2021**, *13*, 57–80. [[CrossRef](#)] [[PubMed](#)]
42. Du, B.; Zhu, G.; Liu, S.; Wang, Y.; Yu, B.; Xu, K. Key factors and mechanisms affecting calcite growth and dissolution—a critical review. *Earth Sci. Front.* **2023**, *30*, 335–351.
43. Larsen, K.; Bechgaard, K.; Stipp, S.L.S. The effect of the Ca²⁺ to CO₃^{2−} activity ratio on spiral growth at the calcite (1014) surface. *Geochim. Cosmochim. Acta* **2010**, *74*, 2099–2109. [[CrossRef](#)]
44. Mahrouqi, D.; Vinogradov, J.; Jackson, M.D. Zeta potential of artificial and natural calcite in aqueous solution. *Adv. Colloid Interface Sci.* **2017**, *240*, 60–76. [[CrossRef](#)] [[PubMed](#)]

Disclaimer/Publisher’s Note: The statements, opinions and data contained in all publications are solely those of the individual author(s) and contributor(s) and not of MDPI and/or the editor(s). MDPI and/or the editor(s) disclaim responsibility for any injury to people or property resulting from any ideas, methods, instructions or products referred to in the content.